Available online at www.sciencedirect.com
ScienceDirect
C. R. Physique 10 (2009) 283–296
COMPTES RENDUS PHYSIQUE

Carbon nanotube electronics / Électronique à nanotubes de carbone

Charge transport in carbon nanotubes based materials: a Kubo–Greenwood computational approach

Hiroyuki Ishii [a], François Triozon [b], Nobuhiko Kobayashi [c], Kenji Hirose [d], Stephan Roche [e,f,*]

[a] *National Institute of Advanced Industrial Science and Technology, Tsukuba central 2, 1-1-1 Umezono, Tsukuba, Ibaraki 305-8568, Japan*
[b] *Commissariat à l'Énergie Atomique, Leti-MINATEC, 17, rue des Martyrs, 38054 Grenoble cedex 9, France*
[c] *Institute of Applied Physics, University of Tsukuba, 1-1-1 Tennodai, Tsukuba, Ibaraki 305-8573, Japan*
[d] *Nano Electronics Research Laboratories, NEC Corporation, 34 Miyukigaoka, Tsukuba, Ibaraki 305-8501, Japan*
[e] *Commissariat à l'Énergie Atomique, INAC/SP2M/L_sim, 17, rue des Martyrs, 38054 Grenoble cedex, France*
[f] *Institute for Materials Science, TU Dresden, D-01062 Dresden, Germany*

Available online 13 June 2009

Abstract

In this contribution, we present a numerical study of quantum transport in carbon nanotubes based materials. After a brief presentation of the computational approach used to investigate the transport coefficient (Kubo method), the scaling properties of quantum conductance in ballistic regime as well as in the diffusive regimes are illustrated. The impact of elastic (impurities) and dynamical disorders (phonon vibrations) are analyzed separately, with the extraction of main transport length scales (mean free path and localization length), as well as the temperature dependence of the nanotube resistance. The results are found in very good agreement with both analytical results and experimental data, demonstrating the predictability efficiency of our computational strategy. ***To cite this article: H. Ishii et al., C. R. Physique 10 (2009).***

Résumé

Transport de charge dans les matériaux à base de nanotubes de carbone : approche numérique. Dans cet article, nous présentons une étude numérique du transport quantique dans les nanotubes de carbone. Après une présentation de la technique numérique employée pour calculer les coefficients de transport, nous illustrons les propriétés du transport balistique, puis les effets dus au désordre statique et au désordre dynamique (vibrations du réseau). Les caractéristiques des échelles de transport (libre parcours moyen élastique, longueur de localisation) sont explicitées, ainsi que la dépendance en température de la résistance des nanotubes. Les résultats obtenus sont en très bon accord avec les données expérimentales. ***Pour citer cet article : H. Ishii et al., C. R. Physique 10 (2009).***

Keywords: Charge transport; Static and dynamical disorders; Kubo–Greenwood conductance; Localization; Ballistic transport

Mots-clés : Transport de charges ; Désordres statique et dynamique ; Conductivité de Kubo–Greenwood ; Localisation ; Transport balistique

* Corresponding author.
E-mail addresses: ishii@bk.tsukuba.ac.jp (H. Ishii), Francois.triozon@cea.fr (F. Triozon), nkoba@bk.tsukuba.ac.jp (N. Kobayashi), hirose@frl.cl.nec.co.jp (K. Hirose), stephan.roche@cea.fr (S. Roche).

1631-0705/$ – see front matter
doi:10.1016/j.crhy.2009.04.003

1. Introduction

Carbon nanotubes (CNTs) are fascinating low-dimensional objects [1] that offer a challenging playground to deepen the analysis of quantum phenomena at the nanoscale. Electronic transport is in this context of particular concern [2–4]. Single-walled metallic carbon nanotubes (SWNT) are long ballistic conductors [5,6] owing to the vanishing contribution of backscattering from elastic disorder [7]. Within the Fermi Golden Rule (FGR), whatever the scattering mechanism (elastic and inelastic), the estimated elastic mean free paths usually reach several micrometers provided that the Fermi level is located close enough to the charge neutrality point (CNP). This property has been evidenced experimentally by measuring the conductance of small diameter metallic tubes contacted to Palladium electrodes [8]. Performant ballistic field effect transistors (CNT-FET) have been also fabricated with semiconducting nanotubes [9,10].

Electron–phonon coupling in carbon nanotubes has been intensively investigated theoretically in relation with temperature-dependent resistivity in metallic carbon nanotubes [11], excited-state carrier lifetime [12–14], excitonic physics [15], temperature dependence of the band gap of semiconducting nanotubes [16], superconductivity [17], and phonon-assisted tunneling in the coulomb blockade regime [18]. The understanding of the role of e–ph coupling in physical properties of carbon nanotubes is thus of genuine importance to deepen the unprecedented physical properties of CNTs.

One of the important consequence of e–ph scattering is to restrict ballistic transport to the low bias regime, for which propagating electrons can only be coupled to low-energy acoustic phonon modes [19]. In this regime the experimental temperature dependence of the tube resistance is linear [11], and driven by acoustic phonon modes. The increase of the applied bias potential across the nanotube further promotes the contribution of higher energy (optic) modes which more significantly impact on the tube conduction, resulting in a saturation regime, or a decrease, of the current versus potential depending on the thermalization rate [20–22].

In the high-bias regime, the inelastic scattering length has been first estimated to be in the order of a few tens of nanometers, on the basis of semiclassical transport description. J.-Y. Park and coworkers [21] have deduced some experimental value for inelastic mean free paths ($\ell_{\rm ie}$) in both low and high bias regimes, on the basis of a phenomenological law between the measured conductance and $\ell_{\rm ie}$ following a diffusive regime $G \sim \frac{2e^2}{h}\ell_{\rm ie}/L_{\rm tube}$. At low bias the estimation gives $\ell_{\rm ie} \simeq 1.6$ μm attributed to scattering with acoustic modes ($\ell_{\rm ac}$), whereas for bias voltage in the order of 0.5 Volt $\ell_{\rm ie} \simeq 10$ nm is assigned to inelastic scattering with zone center and zone boundary optic phonons ($\ell_{\rm opt}$, $\ell_{\rm zb}$). Other estimations using semi-classical Monte Carlo models [8] yield $\ell_{\rm ac} \simeq 300$ nm and $\ell_{\rm opt} \simeq 15$ nm for acoustic and optic modes respectively to reproduce experimental fits [22]. On the other hand, within the framework of effective mass formula and deformation potential approximation [19,21], the computed electron–acoustic phonon scattering length gives $\ell_{\rm ac} \simeq 2.4$ μm in the low bias, and $\ell_{\rm opt} \simeq 180$ nm and $\ell_{\rm zb} \simeq 37$ nm in the high bias regime. By applying a Mathiessen rule, a total scattering length of 30 nm has been inferred, but however disagrees with experimental values. To reconciliate theory with experiment a hot phonons scenario was proposed in [23].

The discussion is nonetheless not yet settled, and several fundamental questions about the nature of inelastic quantum transport in these unique objects are still fiercely debated, as well as the validity of the semiclassical description of transport in a non-equilibrium situation with large electron–phonon interaction [23–31].

In this review article, we focus on quantum transport through CNTs in the presence of elastic disorder and e–ph interaction. We will extensively use the MKRT technique [32] which is a real space (order N) computational framework to study the dynamical properties of quantum wavepackets, as well as the corresponding conductance scaling behaviors, within the framework of the Kubo linear response. This method has been successfully used for treating complex transport problems in quasiperiodic systems, quantum Hall effect [33], carbon nanotubes [25–27,34,35], semiconducting nanowires [36,37] or 2D graphene materials [38]. After discussing about the effect of elastic disorder in Section 2, Section 3 will focus on two possible modeling approaches to tackle with time-dependent one-body description of electronic motion in the presence of lattice vibrations. A scheme to solve the associated time-dependent Schrödinger equation as well as quantum transport in the Kubo framework will be reviewed following [25,26]. The calculated temperature dependence and length scaling of the resistance will be shown to well agree with experimental results.

2. The Kubo–Greenwood approach for quantum transport studies

2.1. Conduction mechanisms and conductance scaling

Efficient computational recursion and order N methods have been successfully developed in solid-state physics since their introduction by R. Haydock [39–41]. The recursion methods are based on an eigenvalue approach of Lanczos [42], and rely on the computation of Green's functions matrix elements by continuous fraction expansion, which can be implemented either in real or reciprocal spaces. These techniques are particularly well suited for treating disorder and defect-related problems, and were successfully implemented to tackle with impurity-level calculations in semiconductors using tight-binding approximation [43], or with electronic structure investigations for amorphous semiconductors, transition metals and metallic glasses based on the linear-muffin-tin orbitals [44].

On the other hand, the general electronic transport theory in the linear response regime relies on the approach derived by Ryogo Kubo [45]. In its zero frequency limit, it reduces to the trace of the operator $\delta(E-H)\hat{V}_x\delta(E-H)\hat{V}_x$, that relates the spectral measure operator $\delta(E-H)$ to the velocity operator $\hat{V}_x$. Electronic dc-conductivity is thus seen as a measure of autocorrelation average of wavepackets velocity operators. During the past decade, the implementation of the recursion method in the calculation of the Kubo–Greenwood transport coefficients has been explored [34,35,26]. This approach, optimized over the years, is mainly based on the resolution of the time-dependent Schrödinger equation (TDSE) employing an expansion of the spectral measure onto a basis of orthogonal (typically Chebyshev) polynomials $Q_n(E)$. By doing so, any operator can be expanded within the same basis as

$$\big|\Psi(t)\big\rangle = \exp\left(-i\frac{Ht}{\hbar}\right)\big|\Psi(0)\big\rangle = \sum_{n=0}^{N}\left(\int n(E)e^{-i\frac{Et}{\hbar}}Q_n(E)\,\mathrm{d}E\right)Q_n(H)\big|\psi(0)\big\rangle \tag{1}$$

which allows an efficient and quick resolution of TDSE. Time-dependent diffusion coefficient is defined as

$$D(E_F,t) = \frac{\langle(\hat{x}(t)-\hat{x}(0))^2\rangle_{E_F}}{2t} \tag{2}$$

$$= \frac{1}{2t}\frac{\mathrm{Tr}[\delta(E_F-\hat{H})(\hat{U}^{\dagger}(t)\hat{x}\hat{U}(t)-\hat{x})^2]}{\mathrm{Tr}[\delta(E_F-\hat{H})]} \tag{3}$$

where $\hat{x}$ is the electron position operator along the tube axis in the Schrödinger representation. $D(E_F)$ represents the diffusion coefficient at the Fermi energy where $D(E_F,t)$ takes the maximum value. Operator $\hat{U}(t)$ represents the time-evolution operator and is broken up into time steps Δt so that the variation of the Hamiltonian operator becomes small,

$$\hat{U}(t) = \prod_{n=0}^{N-1}\hat{S}\big((n+1)\Delta t, n\Delta t\big) \tag{4}$$

where $\Delta t \equiv t/N$. To compute the time evolution of wave packets in huge systems, the time-evolution operator is expanded using Chebyshev polynomials of the first kind, T_n, and Bessel functions, J_n,

$$\hat{S}(t+\Delta t,t) = e^{i\frac{\hat{H}(t)}{\hbar}\Delta t} \tag{5}$$

$$= \sum_{n=0}^{+\infty} e^{-i\frac{a\Delta t}{\hbar}}h_n i^n J_n\left(-\frac{b\Delta t}{\hbar}\right)T_n\left(\frac{\hat{H}(t)-a}{b}\right) \tag{6}$$

Here, the energy spectrum of $\hat{H}$ has the interval $[a-b,a+b]$, $h_0=1$, and $h_n=2$ $(n\geqslant 1)$. The Chebyshev polynomials obey the following recursive relation:

$$T_{n+1}\left(\frac{\hat{H}-a}{b}\right) = 2\left(\frac{\hat{H}-a}{b}\right)T_n\left(\frac{\hat{H}-a}{b}\right) - T_{n-1}\left(\frac{\hat{H}-a}{b}\right) \tag{7}$$

with $T_0((\hat{H}-a)/b)=1$ and $T_1((\hat{H}-a)/b)=(\hat{H}-a)/b$.

From the obtained diffusion coefficient $D(E_F)$, the one-dimensional resistivity ρ defined by the resistance per unit length [21], the mean free path $\ell_{\rm mfp}$, and the relaxation time τ are computed as follows;

$$\rho \equiv \frac{R}{L} = \frac{h}{2e^2}\frac{v_F}{4}\frac{1}{D(E_F)} \tag{8}$$

$$\ell_{\rm mfp} = \frac{2D(E_F)}{v_F} \tag{9}$$

$$\tau = \frac{2D(E_F)}{v_F^2} \tag{10}$$

The trace in Eq. (3), $\mathrm{Tr}[\delta(E-\hat{H})\cdots]$, is computed by $\sum_n \langle\Psi_n|\delta(E-\hat{H})\cdots|\Psi_n\rangle$, where $|\Psi_n\rangle$ is the initial wave packet. We take the electron transfer energy between π-orbitals γ^0, as 2.5 eV in equilibrium states. The C–C bond length is 0.144 nm and the time step is taken as $\Delta t = 0.41$ fs. Since the Bessel functions of the higher-order terms in Eq. (6) decrease to zero for the small Δt, summing up until the tenth order in Eq. (6) is sufficient for good convergence of the results.

The Kubo conductance is given by $G(E) = e^2\,\mathrm{Tr}[\delta(E_F-\hat{H}]D(E_F)/2L$, which is reduced to the computation of on-diagonal Green's function that are achieved by a continuous fraction expansion. Here, L is the system length. From this methodology, it is possible to analyze all the main conduction mechanisms in the quantum coherent regime in various low-dimensional systems or disordered materials. This includes the following:

- Ballistic regime: $G(E) = (2e^2/h)N_\perp(E)$;
- Diffusive regime: $G(E) = (2e^2/h)\ell_{\rm mfp}/L$;
- Weak localization: $G(E) = \frac{2e^2}{h}\ell_{\rm mfp}/L - \delta G_{\rm WL}$;
- Strong localization: $G(E) = \frac{2e^2}{h}\exp(-\xi/L)$, ξ the so-called localization length that is related to the mean free path,

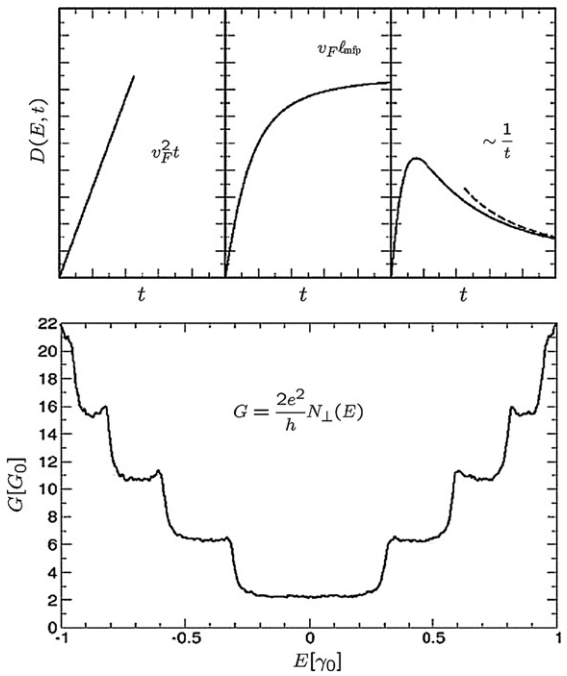

Fig. 1. Top: time-dependent diffusion coefficient for various conduction regimes in metallic carbon nanotubes (10, 10) with or without elastic disorder (Anderson-type). Bottom: quantized energy-dependent Kubo conductance obtained for disorder-free nanotube.

Table 1
Calculated relaxation times, τ, and mean free paths, $\ell_{\rm mfp}$, of the (5, 5)-CNTs using the FGR for several different potential magnitudes, W, and the concentrations, n, of impurities.

	Relaxation time τ [ps]	Mean free path $\ell_{\rm mfp}$ [nm]
$n = 0.05$, $W = 0.3\gamma_0$	0.5	410
$n = 0.10$, $W = 0.3\gamma_0$	0.28	230
$n = 0.05$, $W = 0.6\gamma_0$	0.13	107

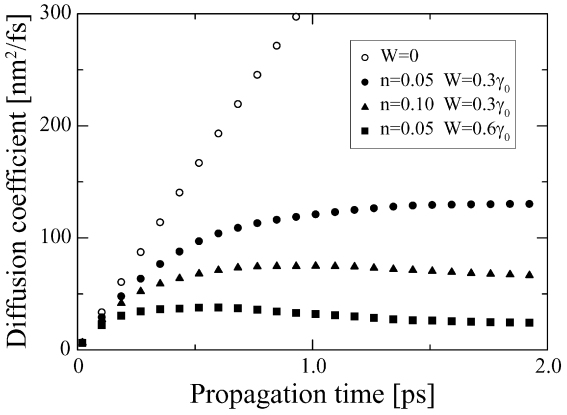

Fig. 2. Calculated time-dependent diffusion coefficients of the (5, 5)-CNTs. White circles indicate the diffusion coefficient of the nanotube without impurities. Black circles, triangles and squares represent the diffusion coefficients for different parameters W and n.

defining $N(E)_\perp$ the conducting channels number, $\ell_{\rm mfp}$ the elastic mean free path associated to a given disorder model, and $\delta G_{\rm WL}$ the weak localization correction to the quantum conductance. In Fig. 1, one shows an illustration of all those conduction mechanisms as well as the obtained conductance for the ballistic case for a metallic (10, 10) nanotube with or without Anderson type disorder (taken as random fluctuations of onsite energies within an interval $[-W/2, W/2]$).

The resistance within a low source-drain bias is also directly obtained from the Kubo formula such as [25,26,46]

$$R(L) = \frac{L}{2e^2}\,\mathrm{Tr}\left[\frac{L}{\delta(E_F - \hat{H})}\right]\frac{1}{D(E_F)} \tag{11}$$

where L is the nanotube length, and $\mathrm{Tr}[\delta(E_F - \hat{H})/L]$ corresponds to the density of states per unit length. The density of states of CNTs at the CNP is $\mathrm{Tr}[\delta(E_F - \hat{H})/L] = 4/hv_F$ where h is the Plank constant and v_F is the Fermi velocity.

2.2. Comparison of elastic scattering times and mean free paths

In this section, we compare the relaxation times using Eq. (10) with those using the Fermi golden rule. We introduce many short-range impurities, $\hat{V}$, randomly in the nanotubes, which changes the on-site energy in our otherwise periodic Hamiltonian form zero to W. The relaxation time using FGR is defined as follows,

$$\frac{1}{\tau} = \frac{2\pi}{\hbar}\left(\sum_f \left|\langle f|\hat{V}|i\rangle\right|^2 N(E_F)\right) \tag{12}$$

where $|i\rangle$ is the initial state at E_F and $|f\rangle$ corresponds to the final states. The density of states is represented by $N(E_F)$. The calculated relaxation times and the mean free paths are shown in Table 1. The impurity concentration, n, is defined as the impurity number divided by the total number of atoms. We can confirm that the relaxation time is inversely proportional to the number of impurities and scales as $1/W^2$.

Fig. 2 shows the time-dependent diffusion coefficients $D(E_F, t)$ for the same Hamiltonians. In case of $n = 0.05$ and $W = 0.3\gamma_0$ (black circles), $D(E_F)$ saturates into about 130 nm^2/fs and from Eqs. (9) and (10) the deduced mean free path and relaxation time are $\ell_{\rm mfp} = 387$ nm and $\tau = 0.47$ ps. For $n = 0.10$ and $W = 0.3\gamma_0$, $\ell_{\rm mfp} = 223$ nm and

$\tau = 0.28$ ps are obtained and $\ell_{\rm mfp} = 113$ nm and $\tau = 0.14$ ps are obtained for $n = 0.05$ and $W = 0.6\gamma_0$. We can confirm that these results well agree with those using FGR.

2.3. Energy-dependent mean free path

For an in-depth understanding of disorder effects in low-dimensional systems, the evaluation of the energy-dependence of the elastic mean free path $\ell_{\rm mfp}$ is an essential step. With Anderson disorder, an analytical result has been derived [5,6]. By reducing the bandstructure to a two-band approximation, and describing the disorder by the onsite Anderson-type potential, $\ell_{\rm mfp}$ was analytically derived, and found to linearly scale with diameter for a fixed disorder strength W, while at a fixed diameter (note that a (n, m) nanotube has a diameter $d_t = \sqrt{3}a_{\rm cc}\sqrt{n^2 + m^2 + nm}/\pi$), the expected disorder scaling $\ell_{\rm mfp} \sim 1/W^2$ was shown. The analytical derivation of such fundamental length scale requires the calculation of total DoS in the vicinity of Fermi level. The DoS can be generally written as $\rho(E) = {\rm Tr}[\delta(E - \mathcal{H})]$ where the trace has to be developed over a complete basis set, while the application of the FGR yields

$$\frac{1}{2\tau_e(E_F)} = \frac{2\pi}{\hbar}\left|\left\langle \Psi_{n1}(k_F)\middle|\hat{\mathcal{U}}\middle|\Psi_{n2}(-k_F)\right\rangle\right|^2 \rho(E_F) \times N_c N_{\rm Ring} \tag{13}$$

with N_c and $N_{\rm Ring}$, the respective number of pair atoms along the circumference and the total number of rings taken in the unit cell used for diagonalization, whereas the eigenstates at the Fermi level are rewritten as

$$\begin{aligned}
\left|\Psi_{n1,n2}(k_F)\right\rangle &= \frac{1}{\sqrt{N_{\rm Ring}}} \sum_{m=1,N_{\rm Ring}} {\rm e}^{{\rm i}mk_F}\left|\alpha_{n1,n2}(m)\right\rangle \quad \text{with} \\
\left|\alpha_{n1}(m)\right\rangle &= \frac{1}{\sqrt{2N_c}} \sum_{n=1}^{N_c} {\rm e}^{\frac{2{\rm i}\pi n}{N_c}}\left(\left|p_z^A(mn)\right\rangle + \left|p_z^B(mn)\right\rangle\right) \\
\left|\alpha_{n2}(m)\right\rangle &= \frac{1}{\sqrt{2N_c}} \sum_{n=1}^{N_c} {\rm e}^{\frac{2{\rm i}\pi n}{N_c}}\left(\left|p_z^A(mn)\right\rangle - \left|p_z^B(mn)\right\rangle\right)
\end{aligned} \tag{14}$$

while the disorder considered here is an uncorrelated white noise (Anderson-type) distribution given by

$$\begin{aligned}
\left\langle p_z^A(mn)\middle|\hat{\mathcal{U}}\middle|p_z^A(m'n')\right\rangle &= \varepsilon_A(m,n)\delta_{mm'}\delta_{nn'} \\
\left\langle p_z^B(mn)\middle|\hat{\mathcal{U}}\middle|p_z^B(m'n')\right\rangle &= \varepsilon_B(m,n)\delta_{mm'}\delta_{nn'} \\
\left\langle p_z^A(mn)\middle|\hat{\mathcal{U}}\middle|p_z^B(m'n')\right\rangle &= 0
\end{aligned} \tag{15}$$

where $\varepsilon_B(m,n)$ and $\varepsilon_A(m,n)$ are the onsite energies of electron at atoms A and B in position (m,n), randomly distributed within the interval $[-W/2, W/2]$ and following some uniform distribution with probability $\mathcal{P} = 1/W$. Then by replacing Eq. (14) in Eq. (13), using Eq. (15), a straightforward calculation gives:

$$\frac{1}{\tau_e(E_F)} = \frac{\pi\rho(E_F)}{\hbar}\left(\frac{1}{\sqrt{N_c N_{\rm Ring}}}\sum_{N_c N_{\rm Ring}} \varepsilon_A^2 + \frac{1}{\sqrt{N_c N_{\rm Ring}}}\sum_{N_c N_{\rm Ring}} \varepsilon_B^2\right)$$

Hence, if the disorder is described by random fluctuations of onsite energies with uniform probability $1/W$ (W the disorder bandwidth) the mean free path can be finally analytically [4,5] derived as

$$\ell_{\rm mfp} = \frac{18a_{\rm cc}\gamma_0^2}{W^2}\sqrt{n^2 + m^2 + nm} \sim \left(\frac{\gamma_0}{W}\right)^2 d_t$$

For the armchair $m = n = 5$ nanotube, with disorder $W = 0.2\gamma_0$, applying the above equation, one finds $\ell_{\rm mfp} \sim$ 560 nm which is much more larger than the circumference length. As shown in Fig. 3, numerical studies [34] confirm the scaling law of the mean free path with the nanotube diameter close to the charge neutrality point. For semiconducting bands, the $1/W^2$ is still satisfied, but mean free paths are seen to be much smaller and do not scale with diameter, in full agreement with experimental measurements [47].

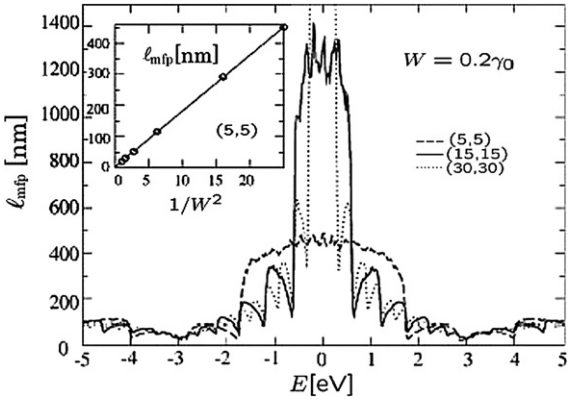

Fig. 3. Main frame: Energy-dependent mean free path as a function of diameter. Insert: $1/W^2$-scaling in agreement with Fermi golden rule. Adapted from [34].

3. Phonon-induced time-dependent Hamiltonian and Kubo conductance

To investigate the effect of electron–phonon coupling on charge transport, an interesting starting point is the Kubo approach of the electronic conductance. The coupling of electrons to the vibrational modes can be encoded into the Hamiltonian by computing the time-dependent quantum dynamics of electronic wavepackets (for π-electrons), under the action of a time-dependent Hamiltonian that mimics the atomic distortions in real space, as well as the strength of e–ph coupling [25,26].

Two approaches have been investigated. The first one is to select phonon modes (acoustic or optic), and to solve the time-dependent Schrödinger equation (TDSE) by splitting the total elapsed time into finite intervals during which the energetics is given by a frozen Hamiltonian. Then, within the Kubo formalism and framework, the conductance scaling can be studied and, for low-energy electrons, the energy-dependent coherence length scaling can be extracted from the conventional weak localization phenomenology [35].

The other approach is to use classical molecular dynamics for describing the time-dependent hopping terms [27]. Using the time-dependent Hamiltonian, the calculation of the time-evolution of wave-packets allow a direct evaluation of the temperature and channel-length dependence of the tube resistance. The mean free path and relaxation time are also obtained. This second approach is more suitable to describe the phenomenology of a thermal bath and thus provide an easier access to temperature-dependent transport properties (in both low and high temperature regimes).

3.1. Approach 1

The real space resolution of the TDSE is achieved as follows [25]. The initial starting Hamiltonian is the π-effective model:

$$\hat{\mathcal{H}}_{\text{eff}} = \sum_i \varepsilon_i |\pi_i\rangle\langle\pi_i| + \sum_{i,\delta=1,3} \gamma(r_{i,i+\delta})\big(|\pi_i\rangle\langle\pi_{i+\delta}| + \text{h.c.}\big) \tag{16}$$

where onsite energies are either all set to zero in absence of elastic disorder, or taken at random within the interval $[-W/2, W/2]$, when simulating an elastic disorder (Anderson-type disorder). The overlap integrals between $|\pi_i\rangle$ and $|\pi_{i+\delta}\rangle$ orbitals are restricted to first neighbors and are given by $\gamma_{i,i+\delta} = \gamma_0$ for all pairs in the case with zero phonons. The effect of phonon vibrations and e–ph couplings is further included by assuming that propagating wavepackets will suffer from a time-dependent change of the electronic energetics ($\gamma_{i,i+\delta}$-matrix) of the underlying effective Hamiltonian. In a weakly disordered two-dimensional system, similar treatment of time-dependent perturbation in the weak localization regime has been shown to correctly reproduce frequency-dependent conductivity corrections [48].

The e–ph interaction is thus encoded through the time-dependent modulation of the hopping interaction, that is $\gamma_0 \to \gamma(r_{i,i+\delta})$, where $r_{i,i+\delta}$ is the bond length. The bond length-dependent Hamiltonian matrix element γ are calculated by using the analytical expression given by D. Porezag et al. [49], that is

$$\gamma(\boldsymbol{r}_{i,i+\delta}) = \gamma\big(\hat{\delta}.\big(\boldsymbol{R}_{i+\delta}(t) - \boldsymbol{R}_i(t)\big)\big) \tag{17}$$

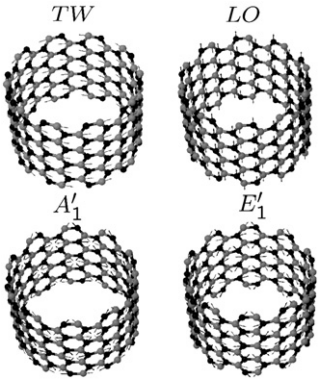

Fig. 4. Representation of phonon polarization vectors for the twist mode (TW) at $q = 0$, together with longitudinal optic (LO) and zone-boundary modes A_1' and E_1'.

where the C–C bond length is $r_{i,i+\delta} = \hat{\delta} \cdot (\mathbf{R}_{i+\delta} - \mathbf{R}_i)$, with $\hat{\delta}$ the bond direction. The atomic positions for a given phonon mode with wave vector $\mathbf{q}$ and frequency $\omega_{\mathbf{q}}$ are given by $\mathbf{R}_i = \mathbf{R}_i^0 + A_\nu(\mathbf{q})\mathbf{e}_\nu(\mathbf{q})\cos(\mathbf{q}.\mathbf{R}_i^0 + \omega_\nu(\mathbf{q})t)$, where $\mathbf{R}_i^0$ are the equilibrium atomic positions, while A, $\mathbf{e}$ and ω are the phonon amplitude, eigenvector and frequency, respectively. As usual, the phonon amplitude can be expressed by [25]

$$A_\nu(\mathbf{q}) = \sqrt{\frac{\hbar n_\nu(\mathbf{q})}{2M_c\omega_\nu(\mathbf{q})}} \tag{18}$$

Here M_c is the carbon mass, while $n_\nu(\mathbf{q})$ is the phonon occupation number for phonon branch ν, as a function of phonon wavevector $\mathbf{q}$. For thermal equilibrium, $n_\nu(\mathbf{q}) = 1/(e^{\hbar\beta\omega_\nu(\mathbf{q})} - 1)$ is the Bose–Einstein occupation factor, $\beta = k_B T$ and $\hbar\omega_\nu(\mathbf{q})$ phonon energy.

The phonon dispersion relations and eigenvectors are computed from the dynamical matrix in a SWNT [50]. Due to the C_N symmetry of the SWNT, the $6N \times 6N$ dynamical matrix is decoupled to N 6×6 matrices (N number of hexagons in a nanotube unit cell) [12]. We then work within the graphene unit cell, which has only one (A, B) atom pair. In the calculations, the z axis is chosen along the tube axis, while the x axis is passing through the A atom in the unit cell. The important phonon modes in the transport of metallic nanotubes are twisting (TW), longitudinal optic (LO), A_1', and E_1' modes, whose frequency are respectively 0, 1596, 1369, and 545 cm^{-1}. The symmetries of these modes are shown in Fig. 4 for illustration.

The phonon polarization vector plays an important role in the e–ph coupling. Amongst the zone-center phonon modes, the LO mode is the one that could most efficiently contribute to inelastic backscattering, whereas among the boundary phonon modes, the dominating contribution comes from the A_1' mode [19,21]. Concerning the TW mode (for $q = 0$), the two atoms of the unit cell move along the same direction along the tube circumference (see Fig. 4). In contrast, for LO mode, the two atoms of the unit cell move one against the other along z axis (see Fig. 4). For A_1' mode, the six atoms on a hexagonal move toward or away the center of the hexagonal (see Fig. 4), whereas for E_1' mode with higher frequency, the tube vibrates like pulling the tube at the two ends.

In our model however, absorption and emission are both assumed to be related to a given amplitude A_0 for a initially thermalized phonon occupation at room temperature, for both LO and A_1' modes. Such hypothesis might not be valid during high-field electron transport, since the high energy phonons excitation rate is faster than their thermalization rate, resulting in a hot phonon generation process [23]. Under such circumstances, one can phenomenologically relax the phonon occupation number in the range of 2–5 [23].

The TDSE is solved by dividing the total evolution time ($t = n\Delta T$) in small time steps ΔT, during which the Hamiltonian energetics is kept constant. This can be expressed as

$$\begin{aligned} \big|\Psi(t)\big\rangle &= \exp\left(-i\frac{\hat{\mathcal{H}}t}{\hbar}\right)\big|\Psi(0)\big\rangle \\ &= \prod_{\alpha=1,n} e^{-iH_\alpha\Delta T}\big|\Psi(0)\big\rangle \end{aligned} \tag{19}$$

where the whole $\gamma_{ij}(\alpha)$ coupling factors as well as onsite energies (defining H_α) will be modified according to the dynamical motion of atomic coordinates defined hereabove. The starting wavepacket is a normalized random phase state that allows efficient treatment of transport in coherent regime. The γ_{ij} terms are modulated by the phonon modes, encoding the information on phonon frequency, polarization vector and amplitude. The chosen time step is about one tenth the oscillation period of the considered phonon mode (given in units of $\hbar/\gamma_0$, so $\Delta T = 1$ corresponds to 0.227 fs). The impact on transport of low energy modes (acoustic TW mode-with time period of 100 fs), and high energy optic modes (with period is 20 fs) have been investigated on both metallic (10, 10) and semiconducting (25, 0) tubes. Typically the chosen time step was $\Delta T = 7(\hbar/\gamma_0) \simeq 1.6$ fs, and the total evolution time $t = 35\,000\hbar/\gamma_0 \sim 10$ ps, giving a length of 5 μm for ballistic transport. For low energy modes, the weak localization phenomenology was discussed [35], whereas the case of optic modes was shown to yield dynamical gaps [25].

3.2. Approach 2

The atomic displacements due to phonon vibrations in real space can be also introduced through the time-dependent electron hopping energies $\gamma(r_{i,i+\delta}(t))$, which is defined as $\gamma(r_{i,i+\delta}(t)) = \gamma^0|\mathbf{R}_i^0 - \mathbf{R}_{i+\delta}^0|^2/|\mathbf{R}_i(t) - \mathbf{R}_{i+\delta}(t)|^2$, where γ^0 is the hopping energy between two nearest-neighbor π orbitals at the equilibrium atomic position $\mathbf{R}^0$. The position at time t is represented by $\mathbf{R}(t)$ [51].

To take the realistic phonon-vibration effects into the transport properties, the motion of carbon atoms can be alternatively obtained by the molecular dynamics simulation using the velocity Verlet algorithm [52],

$$M_c^i \frac{\mathrm{d}^2\mathbf{R}_i}{\mathrm{d}t^2} = -\frac{\mathrm{d}}{\mathrm{d}\mathbf{R}_i}\left\{\sum_{i',j'(>i')}\left[V_R(R_{i'j'}) - \bar{B}_{i'j'}V_A(R_{i'j'})\right]\right\} \tag{20}$$

where M_c^i is mass of ith carbon atom and the distance between ith and jth atoms is represented by R_{ij}. We employ the Brenner–Tersoff potential [53,54] for the repulsive and attractive parts, V_R and V_A. The parameter B_{ij} represents

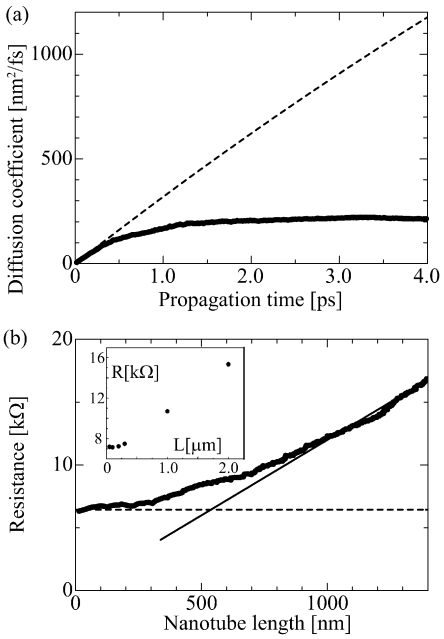

Fig. 5. (a) Calculated diffusion coefficient of the metallic (5, 5)-CNT at the Fermi energy. The straight broken line represents the time-dependent behavior of the diffusion coefficient in case of no scattering effects. Due to the electron–phonon scattering, the diffusion coefficient saturates as shown by bold curve. (b) The resistance as a function of channel-length for the (5, 5)-CNT. Without electron–phonon scattering, the ballistic transport is realized. Therefore, the resistance takes the constant value independent of the nanotube length, as shown by the broken line. The resistance is proportional to the length, when the nanotube is much longer than the mean free path. (Insert) Experimental data of resistance for several channel lengths from [21].

the interaction effect between carbon atoms, for which we use the ones denoted as "Potential II" [53]. The summation runs over all chemical bonds. The phonon dispersion obtained from above formula agrees well with those from other calculations [54,27,55,2], therefore we can treat realistic phonon scattering effects from the present molecular dynamics simulation.

With the molecular dynamics simulations performed for a 100 nm-long nanotube subjected to periodic boundary conditions, we study the transport properties up to the 7.5 μm-long CNTs under open boundary conditions.

4. Channel-length and temperature dependence of the nanotube resistance

To take the realistic phonon-vibration effects on the transport properties into account, we use the phonon modes obtained from the molecular dynamics simulation and study the transport properties of the impurity-free $(5, 5)$-CNTs at the room temperature (300 K).

In the diffusive regime, the time-dependent diffusion coefficient $D(E_F, t)$ of CNT with 7.5 μm length saturates to $D(E_F) = 220\ \text{nm}^2/\text{fs}$ due to electron–phonon scatterings, as shown by the bold curve in Fig. 5(a). We obtain the resistivity $\rho = 12\ \text{k}\Omega/\mu\text{m}$, the mean free path $\ell_{\text{mfp}} = 537$ nm, and the relaxation time $\tau = 654$ fs. We note that the estimated and also experimentally observed mean free path changes from 300 nm to 1.6 μm [21,8] at low bias regime.

In the ballistic regime without any scatterings, the time-dependent behavior of the diffusion coefficient $D(E_F, t)$ increases monotonically as shown by the straight broken line in Fig. 5(a). The slope is equal to $v_F^2 t/2$, since the propagation length of the wave packet, $\sqrt{\langle(\hat{x}(t) - \hat{x}(0))^2\rangle_{E_F}}$, is given by $v_F t$ when electrons pass through the nanotube at the Fermi velocity. $D(E_F, t)$ takes the maximum value at time $t = L/v_F$ and so the diffusion coefficient $D(E_F)$ is proportional to the nanotube length as given by $Lv_F/2$. Using Eq. (11), we obtain the length-independent resistance as $(2G_0)^{-1}$, which corresponds to the inverse of the two conductive channels at the Fermi energy and is consistent with the typical ballistic transport character in Landauer formula. Here, G_0 is defined by $2e^2/h = (12.9\ \text{k}\Omega)^{-1}$.

Next, we consider the nanotube-length dependence of the resistance. The bold curve in Fig. 5(b) shows the resistance as a function of nanotube length. We see that the resistance is equal to the 6.45 kΩ $(= (2G_0)^{-1})$ when the nanotube length is short. On the other hand, when the nanotube length is much longer than the mean free path, electrons are scattered many times by phonons, changing the transport properties into a diffusive character. In this diffusive regime, the resistance is linearly proportional to the nanotube length (Ohm's law) as shown in Fig. 5(b). The straight broken line in Fig. 5(b) represents the ballistic limit of resistance $(2G_0)^{-1}$, while the straight thin line represents the diffusive transport limit. The intersection point of these lines corresponds to the mean free path. It should be noted that the resistance deviates from these lines around the mean free path. As shown in the inset of Fig. 5(b), theoretical and experimental data are fully consistent.

Finally we present the calculated results on the temperature dependence of the resistivity. Fig. 6 shows the one-dimensional resistivity of the $(5, 5)$-CNT as a function of several temperatures in the diffusive transport limit with the nanotube length of 7.5 μm. The resistivity shows linear dependence on the temperature, which is in good agreement qualitatively with experimental observations [11,20] and other theoretical calculation [19].

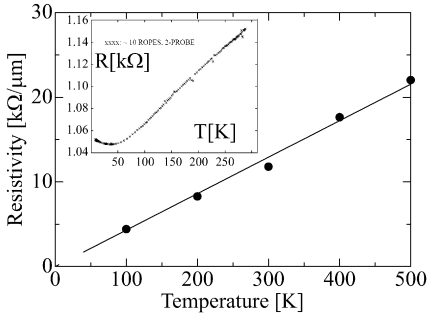

Fig. 6. Calculated resistivities of the $(5, 5)$-CNTs as a function of temperature. We define the resistivity as the resistance per unit length in this work. The resistivity is proportional to the temperature. (Insert) Experimental data of temperature dependence of CNT-bundle resistance from [11].

5. Effect of high-energy phonons within the time-dependent description

The effect of high-energy optic modes on the bandstructure has been first studied by Dubay and coworkers [56]. In their work, a comparison between equilibrium bandstructure and the electronic spectrum of a distorted nanotube, encoding the atomic displacements of high-energy modes, demonstrates the occurrence of shifts of the electronic bands, that scale linearly with the distortion amplitude (see also [13] for armchair tubes).

In [56], the bandstructure changes of a metallic zigzag nanotube (case of $(12, 0)$) due to e–ph coupling was investigated. In the vanishing e–ph coupling situation, the electronic structure shows a very small bandgap due to curvature effects. Then by considering the LO (1591 cm^{-1}), they introduce the relative displacement δd of π orbital position with respect to their equilibrium position (see Fig. 7 top panel). The bandstructures for several values of such scaling parameter are then computed with *ab initio* DFT method. As a result, a bandgap oscillation is found, whose value is reported to follow $\Delta_g = 26\ \text{eV}\,\text{Å}^{-1}|\delta d|$, whereas no detailed information about the rest of the spectrum is given. By using the computational approach introduced in Section 3, we have investigated the time-dependence of the density of states. In Fig. 7, one shows the DoS for the $(10, 10)$ tube (bottom-left) evaluated at time $t \sim 1600$ fs $\sim 80 T_{\text{LO}}$. We show the result for a doubling in amplitude of the phonon mode. Similarly to [56], the doubling of the displacement results in doubling the energy gap, which equals $\Delta_g = 0.302$ eV for A_0. Following the time-dependent of the DoS, we recover a complex modification of the full energy spectrum with shifts of the van-Hove singularities that can not however be easily understood analytically. The case with a semiconducting $(25, 0)$ tube is also shown (bottom-right) for three values of the phonon amplitudes.

Such effect of the time-dependent modulations of the bandstructure are obviously at the origin of subsequent alteration of conductance scaling properties, if scrutinizing its remaining coherent part. This point should be therefore considered with care at the time of using semiclassical transport theories and FGR to describe relevant transport length scales of current-voltage characteristics of CNT-based devices. Within the Kubo framework, the high-energy phonon modes have a strong impact in the conductance even in the linear response regime [25]. This clearly brings some

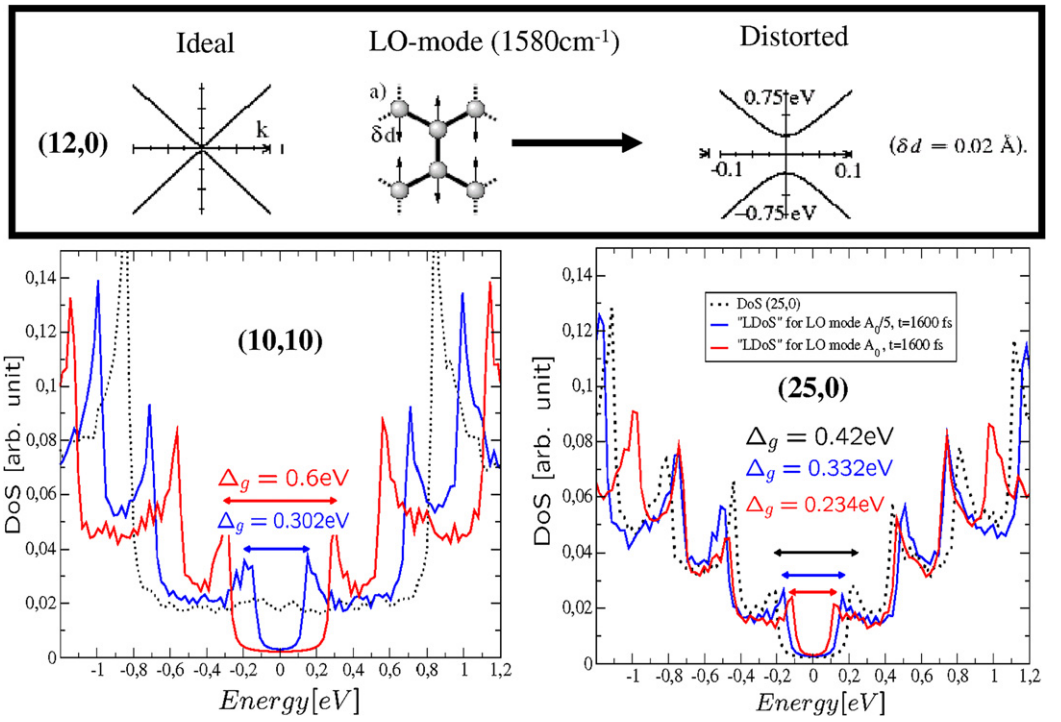

Fig. 7. Top panel: Ab-initio calculation of dynamical effect of the LO mode on the bandstructure (adapted from [56]). Bottom panel: density of states for a metallic $(10, 10)$ tube (left) and a semiconducting $(25, 0)$ tube (right) with e–ph coupling. The effective phonon amplitude is A_0 (blue curve), $2A_0$ (red curve) for the $(10, 10)$ and, $A_0/5$ (blue curve), A_0 (red curve) at $t = 1600$ fs for the $(25, 0)$ case. Dashed lines give the density of states of nanotubes without phonon modulation.

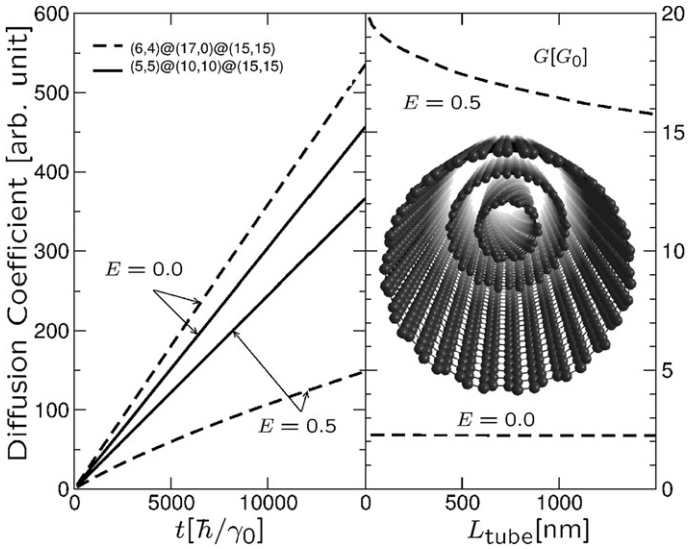

Fig. 8. *Left*: time-dependent diffusion coefficient for incommensurate/commensurate disorder-free MWNTs (with $\beta = \gamma_0/8$). *Right*: length dependence of conductance for two Fermi energies for $(6, 4)@(17, 0)@(15, 15)$.

contradiction in the sense that in this regime (low bias limit) there is no phase space for inelastic processes, which are forbidden by Pauli blocking.

To circumvent such limitation of the Kubo approach, one should notice that within this time-dependent description, the "phonon modes" are intrinsically activated since the atoms are forced to vibrate with a well defined amplitude and phase, whereas the Pauli principle is not properly taken into account in this one-body description. Such approximation of the linear response (Kubo) fully prevents to address high bias voltage regime. Another limitation of this approach is that processes of phonon emission and absorption cannot be rigorously distinguished; at least by keeping a real e–ph interaction Hamiltonian. As a consequence, a zero temperature situation (in which no phonon emission is allowed) cannot be described within this framework. Recently, Foa-Torres and coworkers [30,31] have developed a non-perturbative many body approach to investigate e–ph scattering and inelastic transport. Their calculations predict the occurrence of non-equilibrium energy gaps driven by the coupling between electrons and high symmetry phonon modes (zone center and zone boundary), and which is similar to a dynamical Peierls-type mechanism. Their results explore a non-equilibrium non-perturbative situation (at bias voltages of about 160–250 meV) beyond the reach of [23], much in the spirit of the Peierls–Froehlich mechanism.

6. Incommensurability and anomalous quantum transport in multiwalled carbon nanotubes

Thanks to the order N calculation, we were able to establish a deep connection between spectral and dynamical properties of incommensurate multi-walled nanotubes (MWNTs) [34]. The MWNTs are indeed mostly intrinsic incommensurate objects since, due to registry mismatch between neighboring shells, there are very few cases in which the respective symmetries of individual shells allow a common unit cell for the whole object. In most situations, the unit cell length (along the nanotube axis) ratio between adjacent shells is an irrational number, and the MWNT taken as a whole becomes an incommensurate object.

The study of energy-dependent diffusion coefficients in micron long multiwalled carbon nanotubes with intrinsic incommensurability between neighboring shells, demonstrates that the conduction regime evolves from sub-ballistic to diffusive motion as the Fermi level moves to subbands regions of large density of states, as a consequence of enhanced contribution of the underlying aperiodic potential and multiple scattering phenomena.

In incommensurate systems, such as the $(6, 4)@(17, 0)@(15, 15)$ triple wall nanotube, the energy-dependent anomalous conduction due to geometrical incommensurability-induced aperiodic potential is particularly strong. The region around the charge neutrality point remains almost ballistic, as expected from the suppression of the intershell coupling at low energies due to helicity-determined selection rules [57]. In contrast, the rest of the electronic spectrum

shows a very slow expansion of the wave packet in time. In Fig. 8 ones shows the time-dependent evolution of the diffusion coefficient (left) together with the length dependence of the Kubo conductance (right). $D(E,t)$ either shows anomalously slow diffusion, or saturates at long times. Whenever the saturation limit is reached, a mean free path $\ell_{\mathrm{mfp}}(E)$ for the whole object can be meaningfully extracted. The possibility to get anomalous diffusion and elastic mean free path intrinsically associated to an aperiodic potential of an otherwise clean system stands an unprecedented feature in Condensed Matter Physics. In contrast to quasiperiodic systems as model systems for quasicrystals, the simplified tight-binding description in MWNTs correctly reproduce the electronic bandstructure of real nanotubes, so a quantitative comparison between theory and experiments is in principle possible! Despite recent efforts, the unique transport properties of MWNTs predicted theoretically remain to be experimentally confirmed.

7. Conclusion

To conclude, we have presented an efficient Kubo–Greenwood computational approach allowing the exploration of scattering phenomena in carbon nanotubes in presence of both elastic and dynamical disorders. The method has been shown to provide numerical results in very good agreement with both analytical derivation as well as experimental measurements. Therefore, given its efficient predictability efficiency, its applicability to other complex form of carbon based materials and devices is thus very promising for both material science and advanced nanotechnology.

Acknowledgements

H.I., N.K., and K.H. acknowledge the Next Generation Super Computing Project, Nanoscience Program, MEXT, Japan, and ISSP, University of Tokyo. F.T. and S.R. acknowledge support from the ANR/PNANO ACCENT project funded by the French National Research Agency, the CCRT for supercomputing resources, as well as Jie Jiang, Luis Foa-Torres, Sylvain Latil, Didier Mayou and Riichiro Saito for fruitful discussions. S.R. is indebted to the Alexander Von Humboldt Foundation for financial support.

References

[1] S. Iijima, Nature 354 (1991) 56.
[2] R. Saito, G. Dresselhaus, M. Dresselhaus, Physical Properties of Carbon Nanotubes, Imperial College Press, London, 1998.
[3] S. Roche, Ann. Chim. Sci. Mat. 25 (2000) 529.
[4] J.C. Charlier, X. Blase, S. Roche, Rev. Mod. Phys. 79 (2007) 677.
[5] C.T. White, T.N. Todorov, Nature 393 (1998) 240;
P.L. McEuen, et al., Phys. Rev. Lett. 83 (1999) 5098.
[6] S. Roche, G. Dresselhaus, M.S. Dresselhaus, R. Saito, Phys. Rev. B 62 (2000) 16092.
[7] T. Ando, T. Nakanishi, R. Saito, J. Phys. Soc. Jpn. 67 (1998) 2857–2862.
[8] A. Javey, J. Guo, M. Paulsson, Q. Wiang, D. Mann, M. Lundstrom, H. Dai, Phys. Rev. Lett. 92 (2004) 106804.
[9] J. Appenzeller, M. Radosavljevic, J. Knoch, Ph. Avouris, Phys. Rev. Lett. 92 (2004) 048301;
V. Derycke, R. Martel, J. Appenzeller, Ph. Avouris, Nano Lett. 1 (2001) 453.
[10] A. Javey, J. Guo, Q. Wian, M. Lundstrom, H. Dai, Nature (London) 424 (2003) 654.
[11] C.L. Kane, E.J. Mele, J.E. Fischer, R. Lee, P. Petit, A. Thess, R.E. Smalley, S. Tans, C. Dekker, Europhys. Lett. 41 (1998) 683.
[12] J. Jiang, R. Saito, A. Grüneis, S.G. Chou, Ge.G. Samsonidze, A. Jorio, G. Dresselhaus, M.S. Dresselhaus, Phys. Rev. B 71 (2005) 045417.
[13] T. Hertel, G. Moos, Phys. Rev. Lett. 84 (2002) 5002;
S. Reich, M. Dworzak, A. Hoffmann, C. Thomsen, M.S. Strano, Phys. Rev. B 71 (2005) 033402;
M. Máchon, S. Reich, H. Telg, J. Maultzsch, P. Ordejón, C. Thomsen, Phys. Rev. B 71 (2005) 035416.
[14] V. Perebeinos, J. Tersoff, Ph. Avouris, Phys. Rev. Lett. 94 (2005) 086802.
[15] V. Perebeinos, J. Tersoff, Ph. Avouris, Phys. Rev. Lett. 94 (2005) 027402.
[16] R.B. Capaz, C.D. Spataru, P. Tangney, M.L. Cohen, S.G. Louie, Phys. Rev. Lett. 94 (2005) 036801.
[17] X. Blase, Ch. Adessi, D. Connétable, Phys. Rev. Lett. 93 (2004) 237004;
D. Connétable, G.M. Riganese, J.C. Charlier, X. Blase, Phys. Rev. Lett. 94 (2005) 015503.
[18] S. Sapmaz, P. Jarillo-Herrero, Ya.M. Blanter, C. Dekker, H.S.J. van der Zant, Phys. Rev. Lett. 96 (2006) 026801.
[19] H. Suzuura, T. Ando, Phys. Rev. B 65 (2002) 235412;
R.A. Jishi, M.S. Dresselhaus, G. Dresselhaus, Phys. Rev. B 48 (1993) 11385–11389;
L.M. Woods, G.D. Mahan, Phys. Rev. B 61 (2000) 10651;
G. Pennington, N. Goldsman, Phys. Rev. B 68 (2003) 045426.
[20] Z. Yao, C.L. Kane, C. Dekker, Phys. Rev. Lett. 84 (2000) 2941.
[21] J.-Y. Park, S. Rosenblatt, Y. Yaish, V. Sazonova, H. Ustunel, S. Braig, T.A. Arias, P. Brouwer, P.L. McEuen, Nano Lett. 4 (2004) 517.

[22] E. Pop, D. Mann, J. Cao, Q. Wang, K. Goodson, H. Dai, Phys. Rev. Lett. 95 (2005) 155505.
[23] M. Lazzeri, S. Piscanec, F. Mauri, A.C. Ferrari, J. Robertson, Phys. Rev. Lett. 95 (2005) 236802;
M. Lazzeri, S. Piscanec, F. Mauri, A.C. Ferrari, J. Robertson, Phys. Rev. B 73 (2006) 155426.
[24] M. Georghe, R. Gutierrez, N. Ranjan, A. Pecchia, A. Di Carlo, G. Cuniberti, Europhys. Lett. 71 (2005) 438.
[25] S. Roche, J. Jiang, F. Triozon, R. Saito, Phys. Rev. Lett. 95 (2005) 076803.
[26] H. Ishii, N. Kobayashi, K. Hirose, Phys. Rev. B 76 (2007) 205432.
[27] H. Ishii, N. Kobayashi, K. Hirose, Appl. Phys. Express 1 (2008) 123002.
[28] A. Svizhenko, M.P. Anantram, Phys. Rev. B 72 (2005) 085430.
[29] M.A. Kuroda, A. Cangellaris, J.P. Leburton, Phys. Rev. Lett. 95 (2005) 266803.
[30] L.E.F. Foa Torres, S. Roche, Phys. Rev. Lett. 97 (2006) 076804;
L.E.F. Foa Torres, S. Roche, Appl. Phys. A: Mater. Sci. Process. 86 (2007) 283;
L.E.F. Foa Torres, S. Roche, Phys. Rev. B 75 (2007) 153402.
[31] L.E.F. Foa Torres, R. Avriller, S. Roche, Phys. Rev. B 78 (2008) 035412.
[32] D. Mayou, Europhys. Lett. 6 (1988) 549;
D. Mayou, S.N. Khanna, J. Phys. I, France 5 (1995) 1199;
S. Roche, D. Mayou, Phys. Rev. Lett. 79 (1997) 2518;
F. Triozon, J. Vidal, R. Mosseri, D. Mayou, Phys. Rev. B 65 (2002) 220202.
[33] S. Roche, Phys. Rev. B 59 (1999) 2284.
[34] S. Roche, R. Saito, Phys. Rev. Lett. 87 (2001) 246803;
F. Triozon, S. Roche, A. Rubio, D. Mayou, Phys. Rev. B 69 (2004) 121410;
S. Latil, S. Roche, D. Mayou, J.C. Charlier, Phys. Rev. Lett. 92 (2004) 256805;
S. Latil, F. Triozon, S. Roche, in: NATO Science Series II: Mathematics, Physics and Chemistry, vol. 222, Springer, Netherlands, 2006, pp. 143–165;
Ch. Adessi, S. Roche, X. Blase, Phys. Rev. B 73 (2006) 125414;
R. Avriller, S. Latil, F. Triozon, X. Blase, S. Roche, Phys. Rev. B 74 (2006) 121406.
[35] S. Roche, J. Jiang, F. Triozon, R. Saito, Phys. Rev. B 72 (2005) 113410.
[36] T. Markussen, R. Rurali, M. Brandbyge, A.-P. Jauho, Phys. Rev. B 74 (2006) 245313.
[37] A. Lherbier, M. Persson, Y.M. Niquet, F. Triozon, S. Roche, Phys. Rev. B 77 (2008) 085301.
[38] A. Lherbier, B. Biel, Y.-M. Niquet, S. Roche, Phys. Rev. Lett. 100 (2008) 036803;
A. Lherbier, X. Blase, F. Triozon, Y.-M. Niquet, S. Roche, Phys. Rev. Lett. 101 (2008) 036808.
[39] R. Haydock, in: H. Ehrenreich, F. Seitz, D. Turnbull (Eds.), Solid State Physics, vol. 35, Academic Press, New York, 1980, p. 215.
[40] D.G. Petitfor, D.L. Weaire (Eds.), Recursion Method and its Applications, Springer Series in Solid States Sciences, vol. 58, Springer Verlag, Berlin, 1985;
V.S. Viswanath, G. Müller (Eds.), The Recursion Method: Application to Many-Body Dynamics, Lectures Notes in Physics, vol. 23, Springer Verlag, Berlin, 1994.
[41] T. Hoshi, T. Fujiwara, J. Phys. Soc. Jpn. 72 (2003) 2429;
T. Hoshi, T. Fujiwara, J. Phys.: Condens. Matter 18 (2006) 10787–10802.
[42] C. Lanczos, J. Res. Nat. Bur. Stand. 45 (1950) 255.
[43] D.J. Lohrmann, et al., Phys. Rev. B 40 (1989) 8404.
[44] S.K. Bose, K. Winer, O.K. Andersen, Phys. Rev. B 37 (1988) 6262;
S.K. Bose, et al., Phys. Rev. B 37 (1988) 9955;
S.K. Bose, et al., Phys. Rev. B 41 (1990) 7988.
[45] R. Kubo, J. Phys. Soc. Jpn. 12 (1957) 570;
D. Fisher, P.A. Lee, Phys. Rev. B 23 (1981) 6852.
[46] H. Ishii, N. Kobayashi, K. Hirose, Appl. Surf. Sci. 254 (2008) 7600.
[47] B. Stojetz, C. Miko, L. Forro, Ch. Strünk, Phys. Rev. Lett. 94 (2005) 186802.
[48] H. Watanabe, T. Kawarabayashi, Y. Ono, T. Ohtsuki, J. Phys. Soc. Jpn. 72 (2003) 645;
T. Nakanishi, T. Ohtsuki, T. Kawarabayashi, J. Phys. Soc. Jpn. 66 (1997) 949.
[49] D. Porezag, Th. Frauenheim, Th. Köhler, Phys. Rev. B 51 (1995) 12947.
[50] S. Roche, J. Jiang, L.E.F. Foa-Torres, R. Saito, J. Phys. Condens. Matter 19 (2007) 183203.
[51] W.A. Harrison, Electronic Structure and the Properties of Solids: The Physics of the Chemical Bond, Dover Publications, 1989.
[52] W.C. Swope, H.C. Andersen, P.H. Berens, K.R. Wilson, J. Chem. Phys. 76 (1982) 637.
[53] D.W. Brenner, Phys. Rev. B 42 (1990) 9458.
[54] J. Shiomi, S. Maruyama, Phys. Rev. B 73 (2006) 205420.
[55] H. Ishii, N. Kobayashi, K. Hirose, J. Vac. Sci. Technol. B 27 (2009) 882.
[56] O. Dubay, G. Kresse, H. Kuzmany, Phys. Rev. Lett. 88 (2002) 235506;
O. Dubay, G. Kresse, H. Kuzmany, Phys. Rev. B 67 (2003) 035401.
[57] S. Wang, M. Grifoni, Phys. Rev. Lett. 95 (2005) 266802;
S. Wang, M. Grifoni, S. Roche, Phys. Rev. B 74 (2006) 121407 (RC).